

Diagnosing equilibrium quantum phase transitions via out-of-time-order correlations and multiple quantum coherences

R. J. Lewis-Swan,^{1,2} S. R. Muleady,^{1,2} and A. M. Rey^{1,2}

¹*JILA, NIST, Department of Physics, University of Colorado, Boulder, CO 80309, USA*

²*Center for Theory of Quantum Matter, University of Colorado, Boulder, CO 80309, USA*

(Dated: July 28, 2022)

We propose a new method to characterize equilibrium quantum phase transitions in terms of the spectrum of multiple quantum coherence (MQC) intensities, a special type of out-of-time-order correlation. Using the iconic Lipkin-Meshkov-Glick and transverse-field Ising models as illustrative examples, we show that an abrupt change in coherence and entanglement of the ground state across a quantum phase transition is observable in the MQC spectrum. Furthermore, we develop a robust protocol to obtain the MQC intensities across the ground state phase diagram, which is accessible to a broad range of current experiments as it relies on quasi-adiabatic quenches without the requirement of time-reversing the dynamics.

Introduction: Quantum phase transitions (QPTs) [1] play a central role in many fields of quantum science and have been studied using a variety of tools. Fundamentally, QPTs are signaled by non-analyticity in the energy density of the ground state or a vanishing energy gap between the ground and lowest-excited states in the thermodynamic limit. However, quantum information science has ignited a theoretical push towards characterizing the critical region of a QPT via information-theoretic quantities such as entanglement entropy [2–4], Loschmidt echoes [5, 6], fidelity susceptibility [7–9] and coherence measures [10–14].

In parallel, the past two decades have seen a growing experimental focus on the dynamics of quantum information [15] and non-equilibrium systems [16] as a result of improvements in the technical capabilities of atomic, molecular and optical (AMO) experiments. Of recent note is the study of quantum chaos and information scrambling using so-called out-of-time-order correlations (OTOCs) [17–20]. Already, OTOCs have been adapted to study phenomena beyond their original purview, including the diagnosis of dynamical [21] and equilibrium phase transitions [22, 23]. Motivated by these developments, here we report a new way to characterize drastic changes in coherence and entanglement exhibited by the ground state across a QPT via measurements of the spectrum of multiple quantum coherence (MQC) intensities. This spectrum, first developed in the context of nuclear magnetic resonances [24, 25] and recently related to the Fourier spectrum of a specific family of fidelity OTOCs (FOTOCs) [26–29], can capture fine-grained information about the many-body nature of a quantum state. While the MQC spectrum has been predominantly used to study non-equilibrium dynamics, here we show that it can be a powerful tool to characterize the many-body properties of ground states across a QPT, with scope beyond simple measures like the order parameter or even fidelity susceptibility, and can distinguish quantum phases even in the limit of small system size.

More specifically, in this manuscript we demonstrate that the MQC intensities can diagnose the non-analyticity of a QPT for two paradigmatic models: the Lipkin-Meshkov-Glick (LMG) and the transverse-field Ising (TFI) models. We also discuss a dynamical protocol to obtain FOTOCs and the MQC spectrum of ground states from a pseudo-echo of quasi-adiabatic dynamics. In contrast to prior proposals for measuring FOTOCs, our scheme can be more broadly implemented in experiments as there is no requirement for time-reversal of the coherent dynamics [26, 28, 30–33], nor auxiliary qubits [34–36] or randomized measurements [37, 38]. As a consequence, our results are applicable to a broad range of experimentally-relevant models in AMO and condensed matter physics, with immediate impact for state-of-the-art quantum simulators.

Quantifying Quantum Coherence: The spectrum of MQC intensities is a well-established measure of the coherence of a quantum state [24, 25, 27–29]. The intensities can be defined [27] by first noting that a density matrix $\hat{\rho}$ describing a quantum state can be decomposed into blocks: $\hat{\rho} \equiv \sum_m \hat{\rho}_m$ with $\hat{\rho}_m = \sum_{\lambda_i - \lambda_j = m} \rho_{ij} |\lambda_i\rangle\langle\lambda_j|$. Here, $|\lambda_i\rangle$ are eigenstates of a given Hermitian operator \hat{A} such that $\hat{A}|\lambda_i\rangle = \lambda_i|\lambda_i\rangle$. By construction, the blocks $\hat{\rho}_m$ contain all coherences between eigenstates of \hat{A} differing by m . This coherence is quantified by the MQC intensity $I_m^{\hat{A}}(\hat{\rho}) = \text{Tr}[\hat{\rho}_{-m}\hat{\rho}_m]$, which is a basis-dependent quantity (i.e. depends on the choice of \hat{A}).

The connection between QPTs and the MQC spectrum is fundamentally motivated by similar reasoning to that connecting QPTs to the fidelity [5, 6] and coherence [10] susceptibilities: when a system crosses a QPT the ground state undergoes a drastic change in properties and underlying many-body structure. We argue that this abrupt shift in structure should lead to a sharp change in the features of the MQC spectrum in an appropriate basis.

To formalize our argument, we consider a toy Hamiltonian of a typical QPT: $\hat{H} = \hat{H}_1 + \lambda\hat{H}_2$ with $[\hat{H}_1, \hat{H}_2] \neq 0$ and $\lambda \geq 0$ is a dimensionless (tunable) driving parameter.

ter. Without loss of generality, we take $\hat{A} = \hat{H}_2$ and consider the ground state in the limiting cases $\lambda \rightarrow 0$ and $\lambda \rightarrow \infty$. In the latter case, the ground state $|\psi_{\text{GS}}^{\lambda \rightarrow \infty}\rangle$ of \hat{H} is the lowest-energy eigenstate of \hat{H}_2 , and thus $\hat{\rho}_{\text{GS}}^{\lambda \rightarrow \infty} = |\psi_{\text{GS}}^{\lambda \rightarrow \infty}\rangle\langle\psi_{\text{GS}}^{\lambda \rightarrow \infty}|$ is composed of a single diagonal entry in the eigenbasis defined by $\hat{A} = \hat{H}_2$. Trivially, the MQC spectrum will then be composed of a single peak, $I_m^{\hat{H}_2}(\hat{\rho}_{\text{GS}}^{\lambda \rightarrow \infty}) = \delta_{m,0}$, due to the lack of coherences with respect to \hat{H}_2 . Conversely, for $\lambda \rightarrow 0$ the ground state $|\psi_{\text{GS}}^{\lambda \rightarrow 0}\rangle$ becomes an eigenstate of \hat{H}_1 . As $[\hat{H}_1, \hat{H}_2] \neq 0$ this ground state cannot be a simultaneous eigenstate of \hat{H}_2 : $|\psi_{\text{GS}}^{\lambda \rightarrow 0}\rangle$ must be a coherent superposition of eigenstates of \hat{H}_2 such that the density matrix $\hat{\rho}_{\text{GS}}^{\lambda \rightarrow 0} = |\psi_{\text{GS}}^{\lambda \rightarrow 0}\rangle\langle\psi_{\text{GS}}^{\lambda \rightarrow 0}|$ possesses off-diagonal coherences with respect to the \hat{H}_2 eigenbasis. Consequently, we expect a (relatively) broad MQC spectrum with non-zero $I_m^{\hat{H}_2}(\hat{\rho}_{\text{GS}}^{\lambda \rightarrow 0})$ for $m \neq 0$.

The spirit of this argument can be extended between the two limiting cases, so that we might expect an abrupt change at the critical point λ_c between a narrow to broad spectrum. Given the constraint $\sum_m I_m = 1$ for a pure state [27], this change in width of the spectrum will typically also be observable as a sudden change in the intensity $I_0^{\hat{A}}(\hat{\rho}_{\text{GS}})$. In the following we demonstrate that this is the case and that the width of the spectrum and $I_0^{\hat{A}}(\hat{\rho}_{\text{GS}})$ can serve as experimentally-accessible signatures of a QPT.

Signals of a QPT in MQC spectrum: As an example we consider a pair of iconic models of quantum magnetism: the anisotropic Lipkin-Meshkov-Glick [39, 40] and the one-dimensional transverse-field Ising [41–43] models. The former describes an ensemble of N mutually interacting spin-1/2s in a transverse field, while the latter involves only nearest-neighbour interactions. Each model can be described within the general Hamiltonian

$$\hat{H} = -\frac{1}{2\mathcal{C}} \sum_{i,j} \chi_{ij} \hat{\sigma}_i^z \hat{\sigma}_j^z - \frac{\Omega}{2} \sum_i \hat{\sigma}_i^x, \quad (1)$$

where $\hat{\sigma}_i^\alpha$ are Pauli operators for site i and $\alpha = x, y, z$. The interaction between spins at sites i and j is characterized by χ_{ij} , and Ω is the transverse field strength. We normalize the interaction by $\mathcal{C} = (\sum_{i,j} \chi_{ij}) / \chi N$. For the LMG model $\chi_{ij} = \chi$, while for the TFI model $\chi_{ij} = \chi \delta_{i,j-1}$. We adopt $\hbar = 1$ throughout the manuscript.

Each model features a second-order QPT between ferromagnetic and paramagnetic phases at a critical point $(\Omega/\chi)_c = 1$. The ground state physics can be described within the basis of fully symmetric spin states $|m_\alpha\rangle$ defined by $\hat{S}_\alpha |m_\alpha\rangle = m_\alpha |m_\alpha\rangle$, where $\hat{S}_\alpha \equiv \sum_j (\hat{\sigma}_j^\alpha / 2)$ and we suppress the quantum number $S = N/2$ for brevity. In the strong-field limit $\Omega/\chi \gg 1$ the paramagnetic ground state is characterized by the polarization of all spins identically along \hat{x} , $|\psi_{\text{GS}}^P\rangle = |(N/2)_x\rangle$, while in the

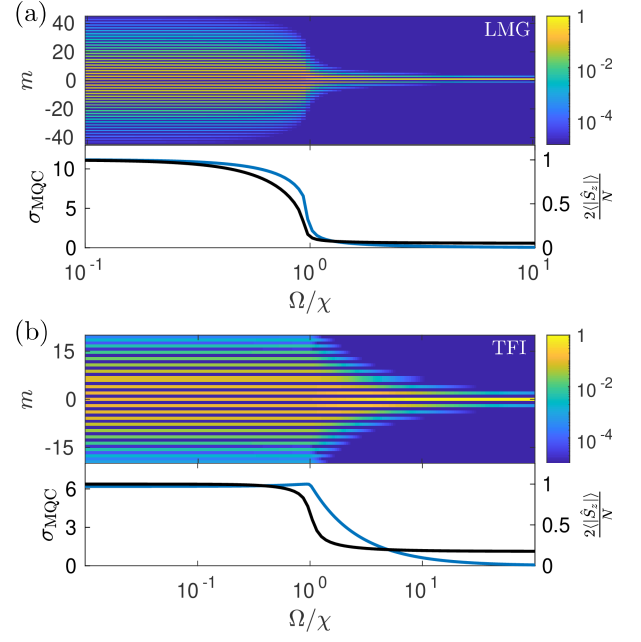


FIG. 1. Characteristic MQC spectra $I_m^{\hat{S}_x}(\hat{\rho}_{\text{GS}})$ of the (a) numerically-computed ground state for the LMG ($N = 250$) and (b) the analytically-computed ground state for the TFI ($N = 20$) models as a function of Ω/χ . The boundary between the ferromagnetic and paramagnetic phases near $\Omega/\chi \approx 1$ is signified by an abrupt change in the slope of the spectrum width, which we quantify in the lower panels using $\sigma_{\text{MQC}}^2 = \sum_m m^2 I_m^{\hat{S}_x}(\hat{\rho}_{\text{GS}})$ (blue). We also compare to the order parameter $\langle |\hat{S}_z| \rangle$ (black).

weak-field limit $\Omega/\chi \ll 1$ the ferromagnetic ground state is an entangled GHZ state $|\psi_{\text{GS}}^F\rangle = |(N/2)_z\rangle \pm |-(N/2)_z\rangle$. We work with the symmetric state, which is adiabatically connected to the paramagnetic ground state for finite N .

To illustrate that the MQC spectrum can serve as a diagnostic tool to distinguish the equilibrium phases, we compute the intensities with respect to the transverse field term in Eq. (1), $\hat{A} = \hat{S}_x$. In Fig. 1 we evaluate the distribution as a function of Ω/χ for $N = 250$ (LMG) and $N = 20$ (TFI). In both cases, deep in the paramagnetic phase the spectrum is dominated by a sharp peak at $I_0 \simeq 1$, which reflects that the ground state $|\psi_{\text{GS}}^P\rangle$ lacks coherences with respect to the eigenstates of \hat{S}_x . Conversely, coherences are generated as the transverse field is reduced relative to the interactions, resulting in the predicted broadening of the MQC spectrum. Quantitatively, the width of the spectrum is defined via $\sigma_{\text{MQC}}^2 = \sum_m m^2 I_m^{\hat{S}_x}(\hat{\rho}_{\text{GS}})$, also known as the curvature, which also serves as a bound on the quantum Fisher information (QFI) [27, 29, 44]. The QPT of each model is then reflected in the abrupt change of the slope of σ_{MQC} near $(\Omega/\chi)_c = 1$. For the TFI model in particular, the change in σ_{MQC} , approaching from $\Omega/\chi < 1$, is sharp even for this small system, and is a much clearer indica-

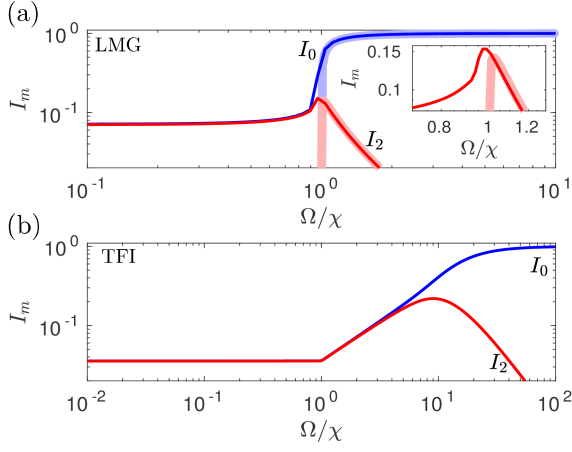


FIG. 2. Signatures of a QPT in the MQC components I_m . (a) The LMG model in the large- N limit (faded lines) predicts that I_0 (blue) and I_2 (red) abruptly vanish at the critical point, $(\Omega/\chi)_c = 1$. The I_2 component develops a sharp peak just upon entering the paramagnetic phase (see inset for magnified view). Dark lines indicate a numerical comparison for $N = 250$. (b) The TFI model predicts a sharp kink in the I_0 and I_2 components at the critical point $(\Omega/\chi)_c = 1$. We plot results for a numerical calculation using $N = 20$.

tion of the transition than the associated order parameter $\langle |\hat{S}_z| \rangle$ of the model.

Formal connections to the QPT are made using analytic solutions for both the LMG and TFI ground states, and consequently the MQC spectrum [45]. For the LMG model analytic expressions are available for $(\Omega/\chi) \leq (\Omega/\chi)_c = 1$ and large N , while the TFI model is tractable in both phases and arbitrary N . In both cases, the MQC intensities are predicted to abruptly change precisely at the QPT $(\Omega/\chi)_c = 1$ [45], as shown in Fig. (2). For $m \neq 0$, the LMG model predicts a sharp peak in $I_m^{\hat{S}_x}(\hat{\rho}_{\text{GS}})$ in the paramagnetic phase. This serves as a clear precursor of the QPT and could be a practical experimental signature. Conversely, the TFI model shows a similar peak but it shifts further into the paramagnetic phase as N increases and is uncorrelated with the QPT.

For finite systems, the location of the transition $(\Omega/\chi)_*$ in the LMG model, signified by a divergence in the derivative $dI_0^{\hat{S}_x}(\hat{\rho}_{\text{GS}})/d\Omega$, approaches the $N \rightarrow \infty$ critical point as $[1 - (\Omega/\chi)_*] \sim N^{-0.57}$ [45]. This is consistent with that of $(\Omega/\chi)_*$ obtained from the susceptibility $d(\sqrt{\langle \hat{S}_z^2 \rangle})/d\Omega$ over the same window of system size N . In contrast, the location of the transition in the TFI model, signified by a discontinuity in the derivative of $dI_0^{\hat{S}_x}(\hat{\rho}_{\text{GS}})/d\Omega$, remains fixed at the critical point regardless of system size.

Collectively, Figs. 1 and 2 demonstrate the utility of the MQC spectrum to diagnose a QPT. Even though the investigated models are of different universality classes, the QPT is unambiguously signalled by an abrupt change

of the spectral width and amplitude of individual MQC intensities in both cases.

Experimental implementation: The Hamiltonian (1) describing the LMG and TFI models can be simulated in state-of-the-art trapped-ion arrays [46–51]. These simulators encode an effective spin-1/2 into the electronic states of each ion, which are then coupled to the collective vibrational modes of the array using an optical dipole force realized by a pair of lasers. This spin-motion coupling mediates effective power-law interactions $\chi_{ij} \propto |r_i - r_j|^{-\alpha}$ with a tunable exponent $0 \leq \alpha \lesssim 3$ [52]. With additional resonant driving of the electronic transition, the LMG model is realized for $\alpha = 0$ and the TFI model is approximated in the limit of large α .

The MQC spectrum can be obtained via a many-body echo protocol, as was recently demonstrated in a trapped ion quantum simulator [49] investigating non-equilibrium dynamics. Fundamental to this is the definition of the intensities in terms of the Fourier transform $I_m^{\hat{A}}(\hat{\rho}) = \sum_{\phi} F_{\phi} e^{im\phi}$ where $F_{\phi} = \text{Tr}[\hat{\rho}\hat{\rho}^{\phi}]$ is the many-body overlap between the reference state $\hat{\rho}$ and the perturbed state $\hat{\rho}^{\phi} \equiv e^{-i\phi\hat{A}}\hat{\rho}e^{i\phi\hat{A}}$. As $\hat{\rho}$ can be a complex many-body state accessing F_{ϕ} is typically experimentally challenging and can require, for example, detailed state tomography [53–56] or randomized measurements [57, 58]. However, obtaining F_{ϕ} is made easier if the state $\hat{\rho}$ is the result of unitary evolution under a controllable Hamiltonian from a simple (e.g. unentangled) initial state.

Specifically, consider $\hat{\rho} = \hat{\rho}(t) = \hat{U}(t)\hat{\rho}_0\hat{U}^{\dagger}(t)$ where $\hat{U}(t)$ describes unitary evolution and $\hat{\rho}_0$ the initial state. We can rewrite $F_{\phi} = \text{Tr}[\hat{\rho}(t)\hat{\rho}^{\phi}(t)] \equiv \text{Tr}[\hat{\rho}_0\hat{\rho}_f^{\phi}]$ where $\hat{\rho}_f^{\phi} \equiv \hat{U}^{\dagger}(t)e^{-i\phi\hat{A}}\hat{U}(t)\hat{\rho}_0\hat{U}^{\dagger}(t)e^{i\phi\hat{A}}\hat{U}(t)$. Hence, F_{ϕ} reduces to a many-body overlap with respect to the initial state $\hat{\rho}_0$ after the many-body echo sequence: i) evolve with $\hat{U}(t)$, ii) perturb with $e^{-i\phi\hat{A}}$, iii) evolve with $\hat{U}^{\dagger}(t)$ [i.e., undo dynamics of i)]. This form of F_{ϕ} realizes a FOTOC [28]. A judicious choice of $\hat{\rho}_0$, such as a product state, then makes accessing the overlap $F_{\phi} = \text{Tr}[\hat{\rho}_0\hat{\rho}_f^{\phi}]$ less demanding.

We propose to obtain the MQC spectrum of the ground state $\hat{\rho}_{\text{GS}}$ for generic Ω/χ by combining the above echo protocol with an adiabatic ramp sequence starting from the paramagnetic ground state $\hat{\rho}_{\text{GS}}^P$ at large field $\Omega/\chi \gg 1$. We illustrate the corresponding many-body echo schematically in Fig. 3(a). The adiabatic sequence, corresponding to $\hat{U}(t)$ in the previous text, entails slowly ramping the Hamiltonian parameters in time such that, starting from $\hat{\rho}(0) = \hat{\rho}_{\text{GS}}^P$ at large $\Omega(0)/\chi \gg 1$ (for simplicity we assume χ is fixed), the instantaneous state of the system follows the ground state of the instantaneous (time-dependent) Hamiltonian $\hat{H}(t)$ characterized by $\Omega(t)/\chi$, $\hat{\rho}(t) \equiv \hat{\rho}_{\text{GS}}(t)$. Ideally, the second half of the many-body echo $[\hat{U}^{\dagger}(t)]$ can be implemented by flip-

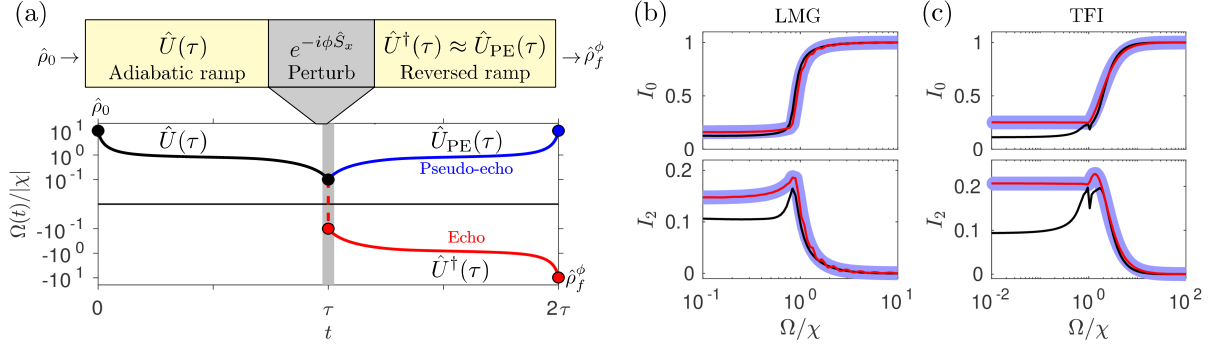


FIG. 3. (a) Schematic of many-body echo to obtain the MQC spectrum. The system is initialized in $\hat{\rho}$, corresponding to the ground state at $\Omega(0)/\chi$, before the field is slowly ramped to $\Omega(\tau)$, described by unitary $\hat{U}(\tau)$. A global rotation is imprinted on the state before the dynamics are reversed via: i) a many-body echo $\hat{U}^\dagger(t)$, or ii) a pseudo-echo $\hat{U}_{PE}(\tau)$. In the former the sign of the Hamiltonian is also flipped, whereas in the latter it is not. (b)-(c) Comparison of LMG and TFI dynamical protocols. The MQC components predicted from the exact ground state (faded blue lines) compared to those obtained from a pseudo-echo ramping sequence of duration $\chi\tau = 10$ (black) and $\chi\tau = 100$ (red). All data is from numerical simulations using $N = 50$ for the LMG model, and $N = 20$ for the TFI model (see Ref. [45] for details of ramps).

ping the sign of the instantaneous Hamiltonian such that $\hat{H}(t) \rightarrow -\hat{H}(2\tau - t)$ for $t > \tau$, where τ is the duration of the initial ramping sequence. Finally, as $\hat{\rho}_{GS}^P$ is a simple product state of all spins pointing along $+\hat{x}$ the overlap with this state can be obtained straightforwardly (e.g. see Ref [50]) to yield F_ϕ .

In a trapped ion simulator the required time-dependent control of a Hamiltonian $\hat{H}(t)$ has already been demonstrated [46, 50, 59]. However, it is not always possible to flip the sign of the interaction (and thus \hat{H}) except for the limiting case of $\alpha = 0$ [45, 52]. Nevertheless, we argue this is not a limitation and the MQC spectrum can still be exactly obtained using a *pseudo-echo* [described by $\hat{U}_{PE}(t)$ in Fig. 3(a)] where the sign of the Hamiltonian is *not* flipped, as long as the ramping sequence is sufficiently adiabatic. Our proof, discussed in detail in Ref. [45], is driven by the observation that the state produced by sequential adiabatic ramps of the transverse field from $\Omega(0) \rightarrow \Omega(t) \rightarrow \Omega(0)$ is effectively identical to that produced by true time-reversal, *i.e.* the system will return to the initial ground state up to an overall irrelevant phase if the dynamics are adiabatic. The fact that the MQC spectrum and thus out-of-time-order correlations are obtainable from coherent dynamics without proper time-reversal can be important in the context of other quantum simulators with similar limitations on control of Hamiltonian parameters.

Numerical example: Realistically, technical constraints and limited ramp durations can preclude the dynamics from being truly adiabatic [60]. Using numerical simulations of small systems, we investigate the effect of these constraints on the obtained MQC spectrum and demonstrate that it retains reliable signatures of the QPT.

In Fig. 3(b)-(c) we present results for both LMG and TFI models for ramps of duration $\chi\tau = (1, 10)$ starting in the paramagnetic phase. For the LMG model we

take $N = 50$ and $\Omega(0) = 10$, while for the TFI model $N = 20$ and $\Omega(0) = 10^2$, with both ramps tailored to reach $\Omega(\tau) = 10^{-2}$ [45]. An important figure of merit is the fidelity with which the targeted ground state is prepared $\mathcal{F} = |\langle\psi_{GS}(\tau)|\psi(\tau)\rangle|^2$. For the respective models the fidelities are: LMG $\mathcal{F} = (0.13, 0.99)$, and TFI $\mathcal{F} = (0.5, 0.99)$. For even low fidelity ramps the intensities obtained from the pseudo-echo reasonably follow the predictions of the exact ground state, despite the generation of appreciable low-energy excitations. As a consequence, when interpreting connections between the MQC spectrum and the quantum phase transition one should demonstrate that the physics observed is dominated by the $T = 0$ ground state. One way to quantify this is to measure a return-fidelity after a pseudo-echo in the absence of the perturbation, which is associated with $\mathcal{F}_{\phi=0}$ (see Ref. [45]). A large return fidelity approaching unity indicates the MQC spectrum is dominated by the ground state contribution.

Conclusion: We have proposed and investigated a novel method to diagnose signatures of a QPT. Our approach is robust and only requires time-dependent control of the Hamiltonian, global rotations and sufficient measurement resolution to distinguish simple product states. Moreover, we demonstrated that the MQC intensities can be reliably obtained from a FOTOC even without the ability to implement proper time-reversal. While our investigation focused on spin models engineered in arrays of trapped ions, our results are broadly applicable to a range of AMO quantum simulators where ground state physics can be studied in a controlled and isolated environment. In particular, we expect neutral atoms in optical lattices in combination with a quantum gas microscope [61] or tweezer arrays [62, 63] should be highly promising platforms for the future.

Acknowledgements: We acknowledge helpful discussions

with Cindy Regal, Mark Brown, and Itamar Kimchi. This work is supported by the AFOSR grant FA9550-18-1-0319, by the DARPA and ARO grant W911NF-16-1-0576, the ARO single investigator award W911NF-19-1-0210, the NSF PHY1820885, NSF JILA-PFC PHY-1734006 grants, and by NIST.

-
- [1] S. Sachdev, *Handbook of Magnetism and Advanced Magnetic Materials* (2007).
 - [2] T. J. Osborne and M. A. Nielsen, *Phys. Rev. A* **66**, 032110 (2002).
 - [3] G. Vidal, J. I. Latorre, E. Rico, and A. Kitaev, *Phys. Rev. Lett.* **90**, 227902 (2003).
 - [4] J. Eisert, M. Cramer, and M. B. Plenio, *Rev. Mod. Phys.* **82**, 277 (2010).
 - [5] H. T. Quan, Z. Song, X. F. Liu, P. Zanardi, and C. P. Sun, *Phys. Rev. Lett.* **96**, 140604 (2006).
 - [6] P. Zanardi and N. Paunković, *Phys. Rev. E* **74**, 031123 (2006).
 - [7] S.-J. GU, *International Journal of Modern Physics B* **24**, 4371 (2010).
 - [8] A. F. Albuquerque, F. Alet, C. Sire, and S. Capponi, *Phys. Rev. B* **81**, 064418 (2010).
 - [9] L. Wang, Y.-H. Liu, J. Imriška, P. N. Ma, and M. Troyer, *Phys. Rev. X* **5**, 031007 (2015).
 - [10] J.-J. Chen, J. Cui, Y.-R. Zhang, and H. Fan, *Phys. Rev. A* **94**, 022112 (2016).
 - [11] G. Karpat, B. Çakmak, and F. F. Fanchini, *Phys. Rev. B* **90**, 104431 (2014).
 - [12] Y.-C. Li and H.-Q. Lin, *Scientific Reports* **6**, 26365 (2016).
 - [13] Y. C. Li, J. Zhang, and H.-Q. Lin, *Phys. Rev. B* **101**, 115142 (2020).
 - [14] M.-L. Hu, Y.-Y. Gao, and H. Fan, *Phys. Rev. A* **101**, 032305 (2020).
 - [15] R. J. Lewis-Swan, A. Safavi-Naini, A. M. Kaufman, and A. M. Rey, *Nature Reviews Physics* **1**, 627 (2019).
 - [16] A. Polkovnikov, K. Sengupta, A. Silva, and M. Vengalattore, *Rev. Mod. Phys.* **83**, 863 (2011).
 - [17] P. Hayden and J. Preskill, *J. High Energy Phys.* , 120 (2007).
 - [18] Y. Sekino and L. Susskind, *J. High Energy Phys.* **2008**, 065 (2008).
 - [19] S. H. Shenker and D. Stanford, *J. High Energy Phys.* **2014**, 67 (2014).
 - [20] A. Kitaev, “In talk at Fundamental Physics Prize Symposium, Nov. 10,” (2014).
 - [21] M. Heyl, F. Pollmann, and B. Dóra, *Phys. Rev. Lett.* **121**, 016801 (2018).
 - [22] H. Shen, P. Zhang, R. Fan, and H. Zhai, *Phys. Rev. B* **96**, 054503 (2017).
 - [23] C. B. Dag, K. Sun, and L.-M. Duan, *Phys. Rev. Lett.* **123**, 140602 (2019).
 - [24] J. Baum, M. Munowitz, A. N. Garroway, and A. Pines, *The Journal of Chemical Physics* **83**, 2015 (1985).
 - [25] P. Cappelaro, in *Quantum state transfer and network engineering* (Springer, 2014) pp. 183–222.
 - [26] M. Gärttner, J. G. Bohnet, A. Safavi-Naini, M. L. Wall, J. J. Bollinger, and A. M. Rey, *Nat. Phys.* , 781 (2017).
 - [27] M. Gärttner, P. Hauke, and A. M. Rey, *Phys. Rev. Lett.* **120**, 040402 (2018).
 - [28] R. J. Lewis-Swan, A. Safavi-Naini, J. J. Bollinger, and A. M. Rey, *Nature Communications* **10**, 1581 (2019).
 - [29] K. Macieszczak, E. Levi, T. Macrì, I. Lesanovsky, and J. P. Garrahan, *Phys. Rev. A* **99**, 052354 (2019).
 - [30] J. Li, R. Fan, H. Wang, B. Ye, B. Zeng, H. Zhai, X. Peng, and J. Du, *Phys. Rev. X* **7**, 031011 (2017).
 - [31] E. J. Meier, J. Ang’ong’a, F. A. An, and B. Gadway, (2017), 10.1103/PhysRevA.100.013623, arXiv:1705.06714.
 - [32] K. X. Wei, C. Ramanathan, and P. Cappelaro, *Phys. Rev. Lett.* **120**, 070501 (2018).
 - [33] G. Zhu, M. Hafezi, and T. Grover, *Phys. Rev. A* **94**, 062329 (2016).
 - [34] B. Swingle, G. Bentsen, M. Schleier-Smith, and P. Hayden, *Phys. Rev. A* **94**, 040302(R) (2016).
 - [35] N. Y. Yao, F. Grusdt, B. Swingle, M. D. Lukin, D. M. Stamper-Kurn, J. E. Moore, and E. A. Demler, “Interferometric approach to probing fast scrambling,” (2016), arXiv:1607.01801.
 - [36] K. A. Landsman, C. Figgatt, T. Schuster, N. M. Linke, B. Yoshida, N. Y. Yao, and C. Monroe, *Nature* **567**, 61 (2019).
 - [37] B. Vermersch, A. Elben, L. M. Sieberer, N. Y. Yao, and P. Zoller, *Phys. Rev. X* **9**, 021061 (2019).
 - [38] M. K. Joshi, A. Elben, B. Vermersch, T. Brydges, C. Maier, P. Zoller, R. Blatt, and C. F. Roos, “Quantum information scrambling in a trapped-ion quantum simulator with tunable range interactions,” (2020), arXiv:2001.02176.
 - [39] H. Lipkin, N. Meshkov, and A. Glick, *Nuclear Physics* **62**, 188 (1965).
 - [40] P. Ribeiro, J. Vidal, and R. Mosseri, *Phys. Rev. Lett.* **99**, 050402 (2007).
 - [41] P. de Gennes, *Solid State Communications* **1**, 132 (1963).
 - [42] R. B. Stinchcombe, *Journal of Physics C: Solid State Physics* **6**, 2459 (1973).
 - [43] A. Dutta, G. Aeppli, B. K. Chakrabarti, U. Divakaran, T. F. Rosenbaum, and D. Sen, *Quantum Phase Transitions in Transverse Field Spin Models: From Statistical Physics to Quantum Information* (Cambridge University Press, 2015).
 - [44] S. L. Braunstein and C. M. Caves, *Phys. Rev. Lett.* **72**, 3439 (1994).
 - [45] “See Supplemental Material at [URL will be inserted by publisher].”.
 - [46] P. Richerme, C. Senko, J. Smith, A. Lee, S. Korenblit, and C. Monroe, *Phys. Rev. A* **88**, 012334 (2013).
 - [47] P. Jurcevic, H. Shen, P. Hauke, C. Maier, T. Brydges, C. Hempel, B. P. Lanyon, M. Heyl, R. Blatt, and C. F. Roos, *Phys. Rev. Lett.* **119**, 080501 (2017).
 - [48] J. Zhang, G. Pagano, P. Hess, A. Kyprianidis, P. Becker, H. Kaplan, A. Gorshkov, Z.-X. Gong, and C. Monroe, “Observation of a many-body dynamical phase transition with a 53-qubit quantum simulator,” (2017), arXiv:1708.01044.
 - [49] M. Gärttner, J. G. Bohnet, M. Safavi-Naini, M. L. Wall, J. J. Bollinger, and A. M. Rey, *Nat. Phys.* **13**, 781 (2017).
 - [50] A. Safavi-Naini, R. J. Lewis-Swan, J. G. Bohnet, M. Gärttner, K. A. Gilmore, J. E. Jordan, J. Cohn, J. K. Freericks, A. M. Rey, and J. J. Bollinger, *Phys. Rev. Lett.* **121**, 040503 (2018).
 - [51] M. L. Wall, A. Safavi-Naini, and A. M. Rey, *Phys. Rev. A* **95**, 013602 (2017).

- [52] K. Kim, M.-S. Chang, R. Islam, S. Korenblit, L.-M. Duan, and C. Monroe, *Phys. Rev. Lett.* **103**, 120502 (2009).
- [53] H. Häffner, W. Hänsel, C. F. Roos, J. Benhelm, D. Chekhal kar, M. Chwalla, T. Körber, U. D. Rapol, M. Riebe, P. O. Schmidt, C. Becher, O. Gühne, W. Dür, and R. Blatt, *Nature* **438**, 643 (2005).
- [54] D. Gross, Y.-K. Liu, S. T. Flammia, S. Becker, and J. Eisert, *Phys. Rev. Lett.* **105**, 150401 (2010).
- [55] B. P. Lanyon, C. Maier, M. Holzäpfel, T. Baumgratz, C. Hempel, P. Jurcevic, I. Dhand, A. S. Buyskikh, A. J. Daley, M. Cramer, M. B. Plenio, R. Blatt, and C. F. Roos, *Nature Physics* **13**, 1158 (2017).
- [56] G. Torlai, G. Mazzola, J. Carrasquilla, M. Troyer, R. Melko, and G. Carleo, *Nature Physics* **14**, 447 (2018).
- [57] A. Elben, B. Vermersch, C. F. Roos, and P. Zoller, *Phys. Rev. A* **99**, 052323 (2019).
- [58] T. Brydges, A. Elben, P. Jurcevic, B. Vermersch, C. Maier, B. P. Lanyon, P. Zoller, R. Blatt, and C. F. Roos, *Science* **364**, 260 (2019).
- [59] J. Cohn, A. Safavi-Naini, R. J. Lewis-Swan, J. G. Bohnet, M. Grttner, K. A. Gilmore, J. E. Jordan, A. M. Rey, J. J. Bollinger, and J. K. Freericks, *New Journal of Physics* **20**, 055013 (2018).
- [60] We note that decoherence will degrade the MQC spectrum, similar to how it limits high-fidelity preparation of the entangled ground state. This specifically motivates our consideration of non-adiabatic ramps, and so we do not specifically calculate the effects of decoherence in this manuscript as it should be a secondary effect in practice.
- [61] C. Gross and I. Bloch, *Science* **357**, 995 (2017).
- [62] A. Keesling, A. Omran, H. Levine, H. Bernien, H. Pichler, S. Choi, R. Samajdar, S. Schwartz, P. Silvi, S. Sachdev, P. Zoller, M. Endres, M. Greiner, V. Vuletic, and M. D. Lukin, *Nature* **568**, 207 (2019).
- [63] A. Browaeys and T. Lahaye, *Nature Physics* **16**, 132 (2020).

Supplemental Material: Diagnosing equilibrium quantum phase transitions via out-of-time-order correlations and multiple quantum coherences

Robert J. Lewis-Swan,^{1,2} Sean R. Muleady,^{1,2} and Ana Maria Rey^{1,2}

¹*JILA, NIST, Department of Physics, University of Colorado, Boulder, CO 80309, USA*

²*Center for Theory of Quantum Matter, University of Colorado, Boulder, CO 80309, USA*

(Dated: July 28, 2022)

I. QUASI-ADIABATIC RAMP SCHEME

In Fig. 3 of the main text we present the multiple quantum coherence (MQC) spectrum of low-energy states obtained as a result of a quasi-adiabatic ramping sequence starting from the paramagnetic ground-state $\hat{\rho}_{\text{GS}}^P$ at large field $\Omega/\chi \gg 1$. To be more specific, we initialize in the fully polarized state $\hat{\rho}_{\text{GS}}^P = |(N/2)_x\rangle\langle(N/2)_x|$ at an initial transverse field $\Omega(0)$ and fixed interaction strength $\chi = 1$. We slowly quench the transverse field over a duration τ down to $\Omega(\tau)$ according to a local adiabatic approximation (LAA) [1, 2] to a final value $\Omega(\tau)$. The MQC spectrum is then obtained via a pseudo-echo which is detailed in the following section.

The LAA ramp sequence entails varying the rate of change $d\Omega/dt$ such that diabatic excitations are created uniformly throughout the ramp. In principle, this is more efficient than, say, a linear ramp with fixed $d\Omega/dt$, for which the performance is greatly determined by excitations generated when the energy gap Δ between ground and excited states is smallest. A LAA ramp can be constructed via

$$\frac{d\Omega}{dt} = \frac{\Delta(t)^2}{\gamma}, \quad (1)$$

$$\gamma = \frac{\tau}{\int_0^{\Omega(\tau)} \frac{d\Omega}{\Delta(B)^2}} \quad (2)$$

where $\Delta(t)$ [$\Delta(\Omega)$] is the energy gap of the instantaneous Hamiltonian (field strength). Example LAA ramps for the Lipkin-Meshkov-Glick (LMG) and 1D transverse-field Ising (TFI) models are shown in Fig. 1.

II. PSEUDO-ECHO PROTOCOL FOR OBTAINING MQC SPECTRUM

In the main text we outline a pair of dynamical protocols [see also Fig. 3(a)] to obtain the MQC spectrum of the ground-state of both TFI and LMG models for a given Ω/χ through an echo or pseudo-echo sequence. We argued that if the ramp dynamics which underly these protocols is sufficiently adiabatic then both sequences are equivalent, i.e., the MQC spectrum and thus related fidelity out-of-time-order correlations from which it is constructed can be obtained without time-reversal of coherent dynamics. In this section we expand upon our reasoning for this connection and provide further justification with numerical simulations of the LMG and TFI models.

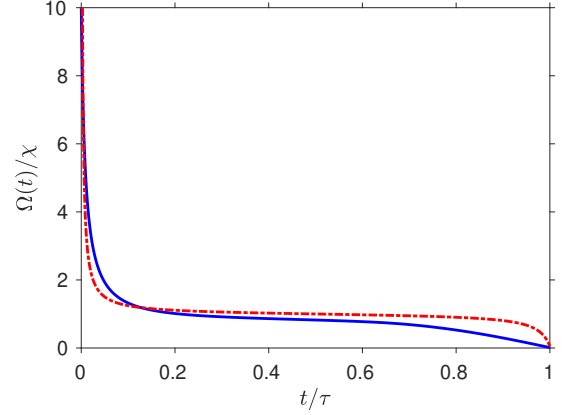


FIG. 1. LAA sequence to ramp down transverse field $\Omega(t)$ for the LMG (solid blue) and TFI (dot-dashed red) models. Examples are for: (LMG) $N = 50$, $\chi\tau = 10$, and $(\Omega(0), \Omega(\tau)) = (10, 10^{-2})$, and (TFI) $N = 20$, $\chi\tau = 10$, and $(\Omega(0), \Omega(\tau)) = (10^2, 10^{-2})$.

A. Connection between ideal and pseudo-echo protocols

Explicitly, the MQC spectrum of the ground-state of both TFI and LMG models for a given Ω/χ can be obtained via an echo sequence. This consists of i) initialization of the spins in the paramagnetic ground-state $\hat{\rho}_0 = |(N/2)_x\rangle\langle(N/2)_x|$ at large initial field $\Omega(0) \gg \chi$, ii) an adiabatic ramp of duration τ wherein the transverse field is slowly quenched to a final value $\Omega(\tau)$ with χ held fixed, iii) a global rotation $\propto e^{-i\hat{\phi}\hat{S}_x}$, and iv) a many-body echo of the initial ramp wherein the sign of the Hamiltonian is flipped and the time-dependence of Hamiltonian parameters is reversed, such that $\hat{H}(t) = -\hat{H}(2\tau - t)$ for $t > \tau$. A measurement of the overlap of the resulting state $\hat{\rho}_f^\phi$ with respect to $\hat{\rho}_0$ for many ϕ then gives access to the MQC spectrum:

$$\begin{aligned} \text{Tr} [\hat{\rho}_0 \hat{\rho}_f^\phi] &\equiv \text{Tr} [\hat{\rho}_0 \hat{U}^\dagger(\tau) e^{-i\phi \hat{S}_x} \hat{U}(\tau) \hat{\rho}_0 \hat{U}^\dagger(\tau) e^{i\phi \hat{S}_x} \hat{U}(\tau)], \\ &= \text{Tr} [\hat{\rho}(\tau) \hat{\rho}^\phi(\tau)], \\ &= \sum_m I_m^{\hat{S}_x}(\hat{\rho}(\tau)) e^{-im\phi}. \end{aligned} \quad (3)$$

Here, we have used the cyclic property of the trace and defined $\hat{\rho}(\tau) = \hat{U}(\tau) \hat{\rho}_0 \hat{U}^\dagger(\tau)$ and $\hat{\rho}^\phi(\tau) = e^{-i\phi \hat{S}_x} \hat{\rho}(\tau) e^{i\phi \hat{S}_x}$ where $\hat{U}(\tau)$ is a unitary operator de-

scribing the ramp evolution. This many-body echo sequence, combined with the measurement $\text{Tr} [\hat{\rho}_0 \hat{\rho}_f^\phi]$, is a type of fidelity out-of-time-order correlation (FOTOC), which were studied in depth in Ref. [3].

Having recapped the ideal echo protocol which allows one to explicitly construct the MQC spectrum of the state $\hat{\rho}(\tau)$ (and thus in principle $\hat{\rho}_{\text{GS}}$), we now discuss in more detail our statement from the main paper wherein we report that the MQC spectrum can also be obtained in the absence of true time-reversal. In particular, we consider the scenario where in step iv) of the ideal echo protocol the sign of the Hamiltonian is not flipped: $\hat{H}(t) = \hat{H}(2\tau - t)$ for $t > \tau$. We term this a *pseudo-echo*. In the following we will i) investigate what information can be extracted when one measures the overlap of the final state of the pseudo-echo $\hat{\rho}_f'^\phi$ with $\hat{\rho}_0$, and ii) formally justify our argument that this measurement precisely gives the MQC spectrum of the ground-state in the limit that the ramping dynamics are adiabatic.

Formally, the overlap with $\hat{\rho}_0$ after the pseudo-echo can be expanded as

$$\begin{aligned} \text{Tr} [\hat{\rho}_0 \hat{\rho}_f'^\phi] &\equiv \text{Tr} [\rho_0 \hat{U}'(\tau) e^{-i\phi \hat{S}_x} \hat{U}(\tau) \rho_0 \hat{U}^\dagger(\tau) e^{i\phi \hat{S}_x} \hat{U}'^\dagger(\tau)], \\ &= \text{Tr} [\hat{\rho}'(\tau) \hat{\rho}^\phi(\tau)], \\ &\equiv \sum_m \tilde{I}_m^{\hat{S}_x}(\hat{\rho}'(\tau), \hat{\rho}(\tau)) e^{-im\phi}. \end{aligned} \quad (4)$$

Here, the second ramp in the pseudo-echo is described by the unitary operator $\hat{U}'(\tau)$, $\hat{\rho}'(\tau) = \hat{U}'^\dagger(\tau) \hat{\rho}_0 \hat{U}'$ and we have defined effective intensities:

$$\tilde{I}_m^{\hat{S}_x}(\hat{\rho}'(\tau), \hat{\rho}(\tau)) \equiv \text{Tr} [\hat{\rho}'_{-m}(\tau) \hat{\rho}_m(\tau)] \quad (5)$$

If $\hat{U}'(\tau) = \hat{U}^\dagger(\tau)$ then we would recover the connection to the MQC spectrum as per Eq. (3), i.e. $\tilde{I}_m^{\hat{S}_x}(\hat{\rho}'(\tau), \hat{\rho}(\tau)) \rightarrow I_m^{\hat{S}_x}(\hat{\rho}(\tau))$.

A pseudo-echo does not realize $\hat{U}'(\tau) = \hat{U}^\dagger(\tau)$ due to the difference in sign of the Hamiltonian $\hat{H}(t)$. However, if the ramping protocol is sufficiently adiabatic, i.e. $\tau \rightarrow \infty$ for a finite system, then it is possible to mimic this relation. To understand this claim, consider a ramp $\hat{U}(\tau \rightarrow \infty)$ which *adiabatically* transforms the initial ground-state $|\psi_{\text{GS}}(0)\rangle$ of $\hat{H}(0)$ into $|\psi_{\text{GS}}(\tau)\rangle$ for $\hat{H}(\tau)$. Then, implement a subsequent adiabatic ramp back to $\hat{H}(2\tau) = \hat{H}(0)$ described by $\hat{U}'(\tau \rightarrow \infty)$. Clearly, if the last ramp is adiabatic then we expect $|\psi_{\text{GS}}(2\tau)\rangle = \hat{U}'(\tau \rightarrow \infty) |\psi_{\text{GS}}(\tau)\rangle \propto |\psi_{\text{GS}}(0)\rangle$ up to an irrelevant global phase. This suggests that $\hat{U}'(\tau \rightarrow \infty) \simeq \hat{U}^\dagger(\tau \rightarrow \infty)$ up to some irrelevant phase. Thus, *if the ramps are adiabatic* then $\tilde{I}_m^{\hat{S}_x}(\hat{\rho}'(\tau), \hat{\rho}(\tau)) \rightarrow I_m^{\hat{S}_x}(\hat{\rho}(\tau))$ and hence the pseudo-echo protocol can be used to obtain the MQC spectrum.

B. Numerical simulations

We verify this statement with numerical simulations of the ideal many-body echo and pseudo-echo protocols for the LMG and TFI models, summarized in Fig. 2. By varying the total ramp duration τ for a small system (LMG $N = 50$, TFI $N = 20$) we are able to evaluate the performance of the pseudo-echo protocol as a function of the adiabaticity of the ramp. We observe that, typically, the effective MQC intensities $\tilde{I}_m^{\hat{S}_x}$ rapidly approach the true intensities $I_m^{\hat{S}_x}$, with increasing τ . An exception is the $m = 0$ intensity for the LMG model, which we find precisely agrees $\tilde{I}_0^{\hat{S}_x} = I_0^{\hat{S}_x}$. This is due to a symmetry possessed by both the LMG and TFI models, as well as the lack of degeneracy in the LMG Hamiltonian, and is discussed in the following subsection. The associated adiabaticity of the ramp, quantified by the fidelity \mathcal{F} of the dynamically prepared state to the equivalent ground-state at $\Omega(\tau)/\chi$, demonstrates that when $\mathcal{F} \gtrsim 0.7$ excellent agreement is found between the two MQC intensities. For completeness, we also plot the return fidelity \mathcal{F}_{ret} , which was introduced in the main text. This quantity is obtained by measuring the overlap of the final and initial states of the pseudo-echo protocol in the absence of any perturbation ($\phi = 0$). The return fidelity serves as a useful way to operationally determine the adiabaticity of the ramps. In this context, one subtlety which must be dealt with properly is that \mathcal{F}_{ret} is only useful as a proxy for \mathcal{F} when $\chi\tau$ is greater than the characteristic time-scale of interactions in the model: $\chi\tau \gtrsim \sqrt{N}$ and $\chi\tau \gtrsim 1$ for the LMG and TFI models, respectively. This is because for shorter ramps no appreciable dynamics can occur, and thus redundantly $\mathcal{F}_{\text{ret}} \sim 1$.

C. Exact connections between MQC intensities due to symmetries of the LMG and TFI model

In the previous subsection, we have established that, excluding the case of adiabatic dynamics, there appears to be no exact correspondence between the MQC intensities obtained from the pseudo-echo and ideal many-body echo protocols in general. However, as hinted at by the results of Fig. (2), in the special case where the dynamics is described by the LMG or TFI models investigated here, and with certain further assumptions, it is actually possible to directly relate the effective MQC intensities $\tilde{I}_m^{\hat{S}_x}$ and the true MQC intensities $I_m^{\hat{S}_x}$. This is specifically related to the fact that the generic Hamiltonian

$$\hat{H} = -\frac{1}{2\mathcal{C}} \sum_{i < j} \chi_{ij} \hat{\sigma}_i^z \hat{\sigma}_j^z - \frac{\Omega}{2} \sum_i \hat{\sigma}_i^x, \quad (6)$$

which describes both the TFI ($\chi_{ij} = \chi \delta_{i,j-1}$, so that $\mathcal{C} = 1$) and LMG ($\chi_{ij} = \chi$, so that $\mathcal{C} = N$) models, is real symmetric: $\hat{H}^* = \hat{H}$ where $*$ denotes complex conjugation. In the following, we will explicitly prove

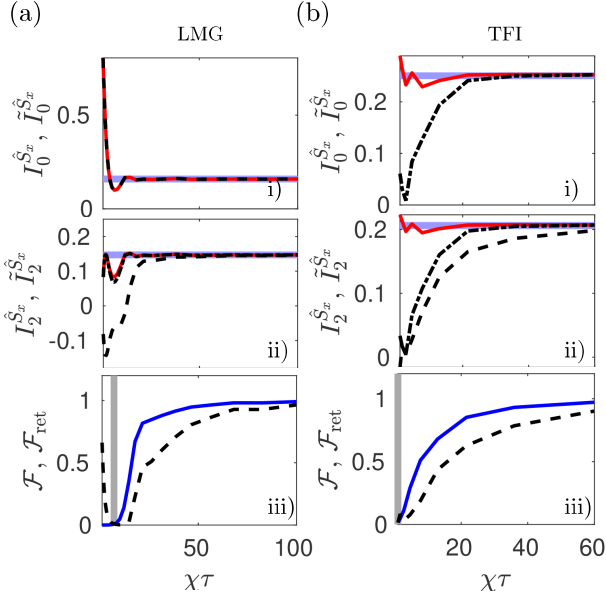


FIG. 2. Evaluation of performance of pseudo-echo in obtaining the MQC spectrum, as compared to the ideal echo protocol, for (a) LMG and (b) TFI models. Intensities are computed for fixed $\Omega(\tau)/\chi = 10^{-2}$. Panels (i)-(ii) Comparison of ideal $I_m^{\hat{S}_x}$ of exact ground-state (thick blue), adiabatic ramp with ideal echo (red) and $\tilde{I}_m^{\hat{S}_x}$ obtained from a pseudo-echo (dashed black). We also plot $|\tilde{I}_m^{\hat{S}_x}|$ (dot-dashed black) which shows improved agreement. Note that in (a), $\tilde{I}_0^{\hat{S}_x} = I_0^{\hat{S}_x}$ due to the symmetries of the LMG model (see text). Panel (iii) Correlation of return fidelity \mathcal{F}_{ret} (dashed black) with fidelity \mathcal{F} (solid blue) of prepared state to the actual ground-state (for $\Omega(\tau) = 10^{-2}$) as a function of ramp duration τ . Vertical grey line indicates characteristic interaction timescales $\chi\tau = \sqrt{N}$ (LMG) and $\chi\tau = 1$ (TFI) (see text).

this results in a connection between $\tilde{I}_m^{\hat{S}_x}$ and $I_m^{\hat{S}_x}$ for the LMG model, including the result that $\tilde{I}_0^{\hat{S}_x} = I_0^{\hat{S}_x}$, and then comment on the implications for the TFI model.

1. Connection for ramping protocol

We consider a toy model of the ramping sequences described by $\hat{U}(\tau)$ and $\hat{U}^\dagger(\tau)$ constructed by discretizing them into $j = 1, 2, \dots, n$ steps of duration $\Delta\tau = \tau/n$ each described by the instantaneous LMG Hamiltonian (Eq. (6) with $\mathcal{C} = N$ and $\chi_{ij} = \chi$) $\hat{H}_n \equiv \hat{H}((n-1/2)\Delta\tau)$:

$$\begin{aligned}\hat{U}(\tau) &= \lim_{n \rightarrow \infty} \left[e^{-i\hat{H}_n \Delta\tau} e^{-i\hat{H}_{n-1} \Delta\tau} \dots e^{-i\hat{H}_2 \Delta\tau} e^{-i\hat{H}_1 \Delta\tau} \right], \\ \hat{U}^\dagger(\tau) &= \lim_{n \rightarrow \infty} \left[e^{-i\hat{H}_1 \Delta\tau} e^{-i\hat{H}_2 \Delta\tau} \dots e^{-i\hat{H}_{n-1} \Delta\tau} e^{-i\hat{H}_n \Delta\tau} \right].\end{aligned}\quad (7)$$

As will become clear, it is also useful to note that in this model also

$$\hat{U}^\dagger(\tau) = \lim_{n \rightarrow \infty} \left[e^{i\hat{H}_n \Delta\tau} e^{i\hat{H}_{n-1} \Delta\tau} \dots e^{i\hat{H}_2 \Delta\tau} e^{i\hat{H}_1 \Delta\tau} \right]. \quad (8)$$

Trivially, for an initial pure state $|\psi(0)\rangle$ we have that $\hat{\rho}(\tau) = |\psi(\tau)\rangle\langle\psi(\tau)|$ with $|\psi(\tau)\rangle = \hat{U}(\tau)|\psi(0)\rangle$, and similarly $\hat{\rho}'(\tau) = |\psi'(\tau)\rangle\langle\psi'(\tau)|$ with $|\psi'(\tau)\rangle = \hat{U}^\dagger(\tau)|\psi(0)\rangle$.

A consequence of \hat{H}_j being real symmetric is that any associated evolution is complex symmetric: i.e., $(e^{-i\hat{H}_j \Delta\tau})^\dagger \equiv (e^{-i\hat{H}_j \Delta\tau})^* = e^{i\hat{H}_j \Delta\tau}$. If we assume that the initial state can be expanded in the fully symmetric Dicke basis as $|\psi(0)\rangle = \sum_m c_m(0)|m_x\rangle$ with $c_m(0) \in \mathbb{R}$ then the fact that the unitary operator is complex symmetric leads us to the useful result $|\psi'(\tau)\rangle = \sum_m c_m^*(\tau)|m_x\rangle$ and $|\psi(\tau)\rangle = \sum_m c_m(\tau)|m_x\rangle$. The fact that the two states $|\psi'(\tau)\rangle$ and $|\psi(\tau)\rangle$ share the same coefficients up to conjugation allows us to directly relate the MQC intensities:

$$I_m^{\hat{S}_x}(\hat{\rho}) = \sum_n |c_n|^2 |c_{n+m}|^2, \quad (9)$$

$$\tilde{I}_m^{\hat{S}_x}(\hat{\rho}, \hat{\rho}') = \sum_n c_n^2 c_{n+m}^{*2}. \quad (10)$$

From these equations, we can immediately deduce $\tilde{I}_0^{\hat{S}_x} = I_0^{\hat{S}_x}$. Moreover, the form of Eqs. (9) and (10) allow us to establish a bound on curvature $\sum_m m^2 |I_m^{\hat{S}_x}| \geq \sum_m m^2 |\tilde{I}_m^{\hat{S}_x}|$. This inequality has a subsequent practical application as a bound on the quantum Fisher information [4–6] $\mathcal{F}_Q \geq 2 \sum_m m^2 |\tilde{I}_m^{\hat{S}_x}|$.

The results (9) and (10) explain why we explicitly observe $\tilde{I}_0^{\hat{S}_x} = I_0^{\hat{S}_x}$ in Fig. 2 for the LMG model. Moreover, as also evidenced in Fig. 2, we find that $|\tilde{I}_m^{\hat{S}_x}|$ typically follows $I_m^{\hat{S}_x}$ more closely, particularly for ramps which are not adiabatic. In this context, we always plot $|\tilde{I}_m^{\hat{S}_x}|$ in Fig. 3(b)-(c) of the main text.

2. Extension to TFI model

These findings for the LMG model can be extended to the TFI case after appropriately accounting for the degeneracy of states with total spin projection m_x . Specifically, if we expand $|\psi(\tau)\rangle = \sum_{m,\alpha} c_{m,\alpha} |m_x, \alpha\rangle$ where $\hat{S}_x |m_x, \alpha\rangle = m |m_x, \alpha\rangle$ and α labels each degenerate state, then for the TFI model we have the more general results

$$I_m^{\hat{S}_x}(\hat{\rho}) = \sum_{n,\alpha,\alpha'} |c_{n,\alpha}|^2 |c_{n+m,\alpha'}|^2, \quad (11)$$

$$\tilde{I}_m^{\hat{S}_x}(\hat{\rho}, \hat{\rho}') = \sum_{n,\alpha,\alpha'} c_{n,\alpha}^2 c_{n+m,\alpha'}^{*2}. \quad (12)$$

Thus, for the TFI model and for more general models described by the Hamiltonian (6) which probe the full 2^N

Hilbert space, Eqs. (11) and (12) imply that $\tilde{I}_0^{\hat{S}_x} \neq I_0^{\hat{S}_x}$ unlike the LMG model.

III. EXACT SOLUTIONS FOR MQC SPECTRUM

The ground-state, and associated MQC spectrum, can be solved analytically for both the LMG and TFI models. In the following we outline the details of the exact solutions and analytic expressions for the MQC intensities. The results of these calculations are plotted in Figs. 1(b) and 2 of the main text.

A. TFI model

We first focus on the transverse field Ising model in 1D. Assuming periodic conditions (PBC), the TFI model is described by the Hamiltonian

$$\hat{H}_{\text{TFI}} = - \sum_{i=1}^N \hat{\sigma}_i^z \hat{\sigma}_{i+1}^z - g \sum_{i=1}^N \hat{\sigma}_i^x, \quad (13)$$

for Pauli operators $\hat{\sigma}_i^\alpha$, $\alpha = x, y, z$, and where we define the site indices modulo the number of lattice sites, N . This Hamiltonian is equivalent to Eq. (1) of the main text (up to an overall rescaling) for $\chi_{ij} = \chi \delta_{i,j-1}$ so that $\mathcal{C} = 1$, where we imposed periodic boundary conditions and defined $g = \Omega/\chi$ for convenience.

1. Exact ground-state

To find the ground state, we follow the standard procedure of first rotating about the y-axis by an angle $\pi/2$ so that $\hat{\sigma}_i^x \rightarrow -\hat{\sigma}_i^z$, $\hat{\sigma}_i^z \rightarrow \hat{\sigma}_i^x$, and then applying a Jordan-Wigner transformation [7]

$$\hat{\sigma}_i^+ = \hat{c}_i^\dagger e^{i\pi \sum_{j<i} \hat{n}_j}, \quad \hat{\sigma}_i^z = 2\hat{n}_i - 1 \quad (14)$$

with fermionic creation operators \hat{c}_i^\dagger and number operators $\hat{n}_i \equiv \hat{c}_i^\dagger \hat{c}_i$. Thus, our Hamiltonian becomes

$$\begin{aligned} \hat{H}_{\text{JW}} = & - \sum_{i=1}^{N-1} \left(\hat{c}_i^\dagger - \hat{c}_i \right) \left(\hat{c}_{i+1}^\dagger + \hat{c}_{i+1} \right) \\ & + \hat{P} \left(\hat{c}_N^\dagger - \hat{c}_N \right) \left(\hat{c}_1^\dagger + \hat{c}_1 \right) + g \sum_{i=1}^N (2\hat{n}_i - 1) \end{aligned} \quad (15)$$

where $\hat{P} = e^{i\pi \sum_j \hat{n}_j}$ is the fermion number parity operator for the system. For states of odd fermion parity, this Hamiltonian is translationally-invariant and possesses PBC; however, for states of even fermion parity, the Hamiltonian instead possesses anti-periodic boundary conditions (APBC). For both cases, we may write

\hat{H}_{JW} in terms of quasimomentum modes as

$$\begin{aligned} \hat{H}_{\text{JW}} = & - \sum_{k \in \text{B.Z.}} \left[2(\cos k - g) \hat{n}_k \right. \\ & \left. - i \sin k \left(\hat{c}_k^\dagger \hat{c}_{-k}^\dagger - h.c. \right) + g \right] \end{aligned} \quad (16)$$

for fermion number operator $\hat{n}_k = \hat{c}_k^\dagger \hat{c}_k$, where we have substituted $\hat{c}_j = \frac{1}{\sqrt{N}} \sum_{k \in \text{B.Z.}} \hat{c}_k e^{-ijk}$ and assumed a lattice constant $a = 1$ for simplicity. For states with odd fermion parity, the sum over the first Brillouin zone (B.Z.) runs over quasimomentum modes $k = 2\pi n/N$ with integer $n = 0, 1, \dots, N-1$; however, for states with even fermion parity, this sum instead runs over quasimomentum modes $k = 2\pi n/N$ with half-integer $n = 1/2, 3/2, \dots, N-1/2$. For a description of the original physical model, since we have conservation of fermion number parity we can therefore neglect the set of unphysical states corresponding to even (odd) fermion parity states of integer (half-integer) quasimomentum modes.

We now apply a Bogoliubov transformation $\hat{c}_k = u_k \hat{\gamma}_k + i v_k \hat{\gamma}_{-k}^\dagger$ where $u_k = \cos(\theta_k/2)$ and $v_k = \sin(\theta_k/2)$ for some angle θ_k . To conserve particle number, we choose $\tan \theta_k = \sin k / (\cos k - g)$, leaving us with

$$\hat{H}_{\text{Bog}} = \sum_{k \in \text{B.Z.}} \varepsilon_k \hat{\gamma}_k^\dagger \hat{\gamma}_k + E_0 \quad (17)$$

for mode energy

$$\varepsilon_k = 2\sqrt{g^2 - 2g \cos k + 1} \quad (18)$$

and constant offset E_0 which we may neglect.

The ground state of \hat{H}_{Bog} is the vacuum with respect to $\hat{\gamma}_k$, denoted by $|\psi_{\text{GS}}\rangle_\gamma$, and we have an energy gap given by $\varepsilon_0 = 2|g-1|$. This gap vanishes at $g = 1$, indicating a transition between a quantum ferromagnetic phase for $g < 1$ and a quantum paramagnetic phase for $g > 1$. In terms of our original quasimomentum modes, it is straightforward to show

$$|\psi_{\text{GS}}\rangle_\gamma \propto \prod_{0 \leq k < \pi} \left[1 + i \tan(\theta_k/2) \hat{c}_k^\dagger \hat{c}_{-k}^\dagger \right] |0\rangle \quad (19)$$

where $|0\rangle$ is the vacuum with respect to \hat{c}_k and k runs over only half the Brillouin zone to avoid overcounting. Since this state has even parity, the ground state of our original spin model, $|\psi_{\text{GS}}\rangle$, only includes half-integer quasimomentum modes, and thus corresponds exclusively to the ground state of the APBC fermion model. Properly normalizing this state, we arrive at

$$|\psi_{\text{GS}}\rangle = \prod_k \left[\cos(\theta_k/2) + i \sin(\theta_k/2) \hat{c}_k^\dagger \hat{c}_{-k}^\dagger \right] |0\rangle \quad (20)$$

where the product index k is understood is running over only half-integer quasimomentum modes with $0 \leq k < \pi$.

2. FOTOC

To obtain the required MQC spectrum from the ground-state Eq. (20) we must first compute the associated FOTOC. Specifically we compute $F_\phi = \text{Tr} [\hat{\rho}_{\text{GS}} \hat{\rho}_{\text{GS}}^\phi]$ where $\hat{\rho}_{\text{GS}} = |\psi_{\text{GS}}\rangle \langle \psi_{\text{GS}}|$ and $\hat{\rho}_{\text{GS}}^\phi = e^{-i\phi \hat{S}_x} \hat{\rho}_{\text{GS}} e^{i\phi \hat{S}_x}$. The latter is simplified via relating

$$\hat{S}_x = \frac{1}{2} \sum_i \hat{\sigma}_i^x \rightarrow \sum_k \hat{n}_k, \quad (21)$$

and we thus find

$$\begin{aligned} F_\phi &= |\langle \psi_{\text{GS}} | e^{-i\phi \hat{S}_x} | \psi_{\text{GS}} \rangle|^2 \\ &= \prod_k [1 - \sin^2(\phi) f(k, g)] \end{aligned} \quad (22)$$

where $f(k, g) = 1/[1 + (\cos k - g)^2/\sin^2 k]$.

To find an exact closed-form expression for Eq. (22) for arbitrary system size N , we first have that

$$\begin{aligned} 1 - \sin^2(\phi) f(k, g) &= \frac{\sin^2(\phi) \sin^2(k/2)}{g} \\ &\times \frac{[1 - X_{+, \phi}(g)/\sin^2(k/2)] [1 - X_{-, \phi}(g)/\sin^2(k/2)]}{[1 - (-\sinh^2((\ln g)/2))/\sin^2(k/2)]} \end{aligned} \quad (23)$$

for functions

$$\begin{aligned} X_{\pm, \phi}(g) &= \frac{1}{2} \left\{ 1 - \frac{g}{\sin^2(\phi)} \right. \\ &\times \left. \left[1 \mp \sqrt{1 - \sin^2(\phi) \left(1 - \frac{1}{g} \right)^2 + \frac{\sin^4(\phi)}{g^2}} \right] \right\}, \end{aligned} \quad (24)$$

which results from writing (23) as a single rational expression and then factorizing the numerator, which is a quadratic in $\sin^2(k/2)$. Next, we use the following relations [8],

$$\prod_{n=1}^{\lfloor N/2 \rfloor} \sin^2 \left(\frac{(2n-1)\pi}{2N} \right) = \frac{1}{2^{N-1}}, \quad (25)$$

$$\prod_{n=1}^{\lfloor N/2 \rfloor} \left(1 - \frac{\sin^2 z}{\sin^2 \left(\frac{(2n-1)\pi}{2N} \right)} \right) = \begin{cases} \cos(Nz), & N \text{ even} \\ \frac{\cos(Nz)}{\cos z}, & N \text{ odd} \end{cases}, \quad (26)$$

to evaluate the quasimomenta product in (22) using the expression in (24). Assuming that N is even, we thus obtain

$$\begin{aligned} F_\phi &= \frac{4}{1+g^N} \left(\frac{\sin(\phi)}{2} \right)^N \\ &\times \cos(N \arcsin \sqrt{X_{+, \phi}(g)}) \\ &\times \cos(N \arcsin \sqrt{X_{-, \phi}(g)}). \end{aligned} \quad (27)$$

For the case of odd N , the only difference is that (28) is divided through by an additional factor of $\cos(\arcsin \sqrt{X_{+, \phi}(g)}) \cos(\arcsin \sqrt{X_{-, \phi}(g)})$. We note in passing that for even N , we may alternatively express the cosine expressions in terms of the Chebyshev polynomials as $\cos(N \arcsin \sqrt{X_{\pm, \phi}(g)}) = T_{N/2}(1 - 2X_{\pm, \phi}(g))$, where T_α is the α -th Chebyshev polynomial of the first kind.

It is also useful to obtain a more concise expression for Eq. (28) in the limit of large N , which is equivalent to assuming a continuum of quasimomentum modes. Exponentiating our product in (22) and replacing the resulting sum with an integral, $\sum_k \rightarrow N \int_0^\pi dk/(2\pi)$, then

$$F_\phi \simeq e^{-N\lambda_\phi(g)}, \quad (28)$$

$$\lambda_\phi(g) = - \int_0^\pi \frac{dk}{2\pi} \ln [1 - \sin^2(\phi) f(k, g)]. \quad (29)$$

Let us now define the quantity

$$A_n(g) \equiv \int_0^\pi \frac{dk}{2\pi} f(k, g)^n = \frac{a_n}{2} \begin{cases} \frac{1}{2^{2n}}, & g < 1 \\ \frac{1}{(2g)^{2n}}, & g > 1 \end{cases} \quad (30)$$

for central binomial coefficient $a_n = \binom{2n}{n}$; we thus have that $A_n(g) = (a_n/2) A_1(g)^n$. To now evaluate $\lambda_\phi(g)$, we expand the logarithm in the integrand and perform the k integral on each successive term, finding

$$\lambda_\phi(g) = \sum_{n=1}^{\infty} \frac{a_n}{2n} (\sin^2(\phi) A_1(g))^n. \quad (31)$$

Introducing an auxiliary integral to write each term as

$$\frac{a_n}{2n} (\sin^2(\phi) A_1(g))^n = \lim_{\varepsilon \rightarrow 0} \int_{\varepsilon/4}^{\sin^2(\phi) A_1(g)} \frac{dx}{2x} a_n x^n, \quad (32)$$

we can use the fact that $(1-4x)^{-1/2}$ is the generating function for the central binomial coefficients, i.e. $\sum_{n=0}^{\infty} a_n x^n = (1-4x)^{-1/2}$, to eliminate the infinite sum and perform the integral over x , taking the limit $\varepsilon \rightarrow 0$ at the end to cancel singularities arising from the $n=0$ term. We thus obtain

$$\lambda_\phi(g) = - \ln \left(\frac{1 + \sqrt{1 - 4 \sin^2(\phi) A_1(g)}}{2} \right), \quad (33)$$

and so

$$F_\phi \simeq \begin{cases} \left(\frac{1 + |\cos(\phi)|}{2} \right)^N, & g < 1 \\ \left(\frac{1 + \sqrt{1 - \sin^2(\phi)/g^2}}{2} \right)^N, & g > 1 \end{cases}. \quad (34)$$

3. MQC spectrum

In order to study the behavior of the MQC spectrum at the transition, we first turn to our exact expression for the FOTOC in (28), obtaining a rather simple, exact result for the MQC intensities exactly at the transition. For $g = 1$, from (25) we have $X_{+, \phi}(g = 1) = 0$ and $X_{-, \phi}(g = 1) = -\cot^2(2\phi)$, and from this we have

$$F_\phi|_{g=1} = \sin^N(\phi/2) + \cos^N(\phi/2). \quad (36)$$

Using the Fourier decomposition of the FOTOC, $I_m^{\hat{S}_x} \equiv \sum_\phi F_\phi e^{-im\phi}$ we obtain

$$I_m^{\hat{S}_x}|_{g=1} = \frac{2}{4^N} \binom{2N}{N-m}, \quad (37)$$

for even m , and is 0 otherwise. Thus, independent of system size N the critical point of the TFI model is characterized by a Gaussian (binomial) MQC spectrum.

For MQC intensities in the ferromagnetic phase, we find a much simpler analysis proceeds from using the large- N expression for the FOTOC in (35). In fact, this expression yields a constant MQC spectrum for all $g < 1$, and limits to the exact MQC spectrum (37) found at the critical point. From (35) we obtain (again, assuming m is even)

$$I_m^{\hat{S}_x}|_{g<1} \simeq \frac{1}{4^N} \binom{2N}{N-m} + \frac{2}{\pi 4^N} \sum_{\substack{-N+m \leq j \leq N+m, \\ j \text{ odd}}} \binom{2N}{j+N-m} \frac{(-1)^{(j-1)/2}}{j}. \quad (38)$$

To write this latter term in a more insightful form, we first apply the approximation

$$\binom{2N}{j+N-m} \simeq \frac{4^N}{\sqrt{\pi N}} e^{-(j-m)^2/N}. \quad (39)$$

Since we are generally interested in $m \ll \sqrt{N}$, we may extend the bounds of the sum to $j = \pm\infty$, accumulating an error $\lesssim 2e^{-N}/N$. We then recast our expression as

$$\begin{aligned} & \frac{2}{\pi 4^N} \sum_{\substack{-N+m \leq j \leq N+m, \\ j \text{ odd}}} \binom{2N}{j+N-m} \frac{(-1)^{(j-1)/2}}{j} \\ & \simeq \frac{4e^{-m^2/N}}{\pi \sqrt{\pi N}} \sum_{j \text{ odd}, j>0} \frac{(-1)^{(j-1)/2}}{j} e^{-j^2/N}. \end{aligned} \quad (40)$$

Now, the partial sum for all terms with $j \gtrsim \sqrt{N}$ has an absolute value $\lesssim 1/\sqrt{N}$, and neglecting such terms allows us to make the replacement $e^{-j^2/N} \approx 1$. Using $\sum_{j \text{ odd}} (-1)^{(j-1)/2}/j = \pi/4$, and approximating the first

term in our MQC intensity with a Gaussian, we arrive at the result

$$I_m^{\hat{S}_x}|_{g<1} \simeq \frac{2}{\sqrt{\pi N}} e^{-m^2/N}, \quad (41)$$

which is the large- N equivalent of the exact expression found at the transition.

In the large- N limit, we can also examine some features of the MQC spectrum in the paramagnetic phase as we approach the transition. We now add indices to our FOTOC and MQC intensities specifying the system size, so that we have FOTOC $F_{\phi;N}$ and MQC intensity $I_{0;N}^{\hat{S}_x}$ corresponding to system size N . We can see from the large- N expressions in (35) that $F_{\phi;N} = F_{\phi;1}^N$, though we emphasize that this is strictly a mathematical relationship, and we do not expect the large- N expression for $F_{\phi;1}$ to be a good approximation to the exact FOTOC in (28). Motivated by this, we can form a generating sequence for $I_{0;N}^{\hat{S}_x}$ via

$$\begin{aligned} I_0^{\hat{S}_x}(x) & \equiv \sum_{N=0}^{\infty} x^N I_{0;N}^{\hat{S}_x} = \sum_{N=0}^{\infty} x^N \int_0^{2\pi} \frac{d\phi}{2\pi} F_{\phi;N} \\ & = \int_0^{2\pi} \frac{d\phi}{2\pi} \sum_{N=0}^{\infty} x^N F_{\phi;1}^N = \int_0^{2\pi} \frac{d\phi}{2\pi} \frac{1}{1 - x F_{\phi;1}}, \end{aligned} \quad (42)$$

where x is the generating sequence indeterminate. Solving this integral, and taking the derivative with respect to g yields

$$\begin{aligned} \frac{d}{dg} I_0^{\hat{S}_x}(x) & = \frac{x^2(2-x)}{\sqrt{1-x} [4(1-x)g^2 + x^2]^{3/2}} \\ & + \frac{x}{\pi g(1-x) [4(1-x)g^2 + x^2]} \left\{ 4(1-x)(g^2-1)K\left(\frac{1}{g^2}\right) \right. \\ & \left. - 4(1-x)g^2 E\left(\frac{1}{g^2}\right) + (2-x)^2 \Pi\left(\frac{-x^2}{4(1-x)g^2}, \frac{1}{g^2}\right) \right\} \end{aligned} \quad (43)$$

for complete elliptic integral of the first, second, and third kind $K(k)$, $E(k)$, and $\Pi(n, k)$, respectively, where k is the eccentricity and n is the characteristic. Only keeping singular terms in g as g approaches 1 from the paramagnetic side of the transition,

$$\frac{d}{dg} I_0^{\hat{S}_x}(x)|_{g \rightarrow 1^+} \simeq -\frac{1}{2\pi} \frac{4x}{(2-x)^2} \ln(1-1/g^2) \quad (44)$$

and by taking the N -th derivative at $x = 0$ and dividing by $N!$, we arrive at

$$\frac{d}{dg} I_{0;N}^{\hat{S}_x}|_{g \rightarrow 1^+} \simeq -\frac{N}{\pi 2^N} \ln(g-1). \quad (45)$$

Despite the logarithmic divergence of this expression as we approach the transition for fixed N , we can also see

that there is an exponential suppression in N , and thus the onset of this divergence is well within the quantum critical regime where one expects the breakdown of large- N expressions.

B. LMG model

The LMG model describes a system of N mutually interacting spin-1/2s and is defined by the Hamiltonian

$$\hat{H} = -\frac{\chi}{N}\hat{S}_z^2 - \Omega\hat{S}_x \quad (46)$$

where we introduced collective spin operators $\hat{S}_\alpha = \sum_j \hat{\sigma}_j^\alpha / 2$ for $\alpha = x, y, z$. This Hamiltonian emerges from Eq. (1) of the main text for $\mathcal{C} = N$ and $\chi_{ij} = \chi$.

1. Ground-state for large N

An exact solution of the ground-state and low-energy physics can be obtained via a Holstein-Primakoff transformation in the large N limit. We follow the derivation previously reported in Ref. [9] and references therein, and summarize the key results here. Specifically, we write the collective spin operators in terms of bosonic operators

$$\begin{aligned} \hat{S}_x &= \frac{N}{2} - \hat{a}^\dagger \hat{a}, \\ \hat{S}_- \equiv \hat{S}_z - i\hat{S}_y &= -(\sqrt{N - \hat{a}^\dagger \hat{a}})\hat{a}. \end{aligned} \quad (47)$$

Using a $1/N$ expansion of the spin raising and lower operators and restricting to the paramagnetic phase ($\Omega \leq 1$) the LMG Hamiltonian (46) can be written as:

$$\hat{H}_{\text{HP}} = \frac{1}{2}(2\Omega - \chi)\hat{a}^\dagger \hat{a} - \frac{\chi}{4}(\hat{a}^2 + \hat{a}^{\dagger 2}). \quad (48)$$

This bosonic Hamiltonian is then diagonalized via the Bogoliubov transformation $\hat{a} = \sinh(r)\hat{b}^\dagger + \cosh(r)\hat{b}$ with $\tanh(2r) = \chi/(2\Omega - \chi)$, such that \hat{H}_{HP} becomes:

$$\hat{H}_{\text{bog}} = \sqrt{\Omega(\Omega - \chi)}\hat{b}^\dagger \hat{b}. \quad (49)$$

The eigenstates of \hat{H}_{bog} are Fock states of the Bogoliubons, $\hat{b}^\dagger \hat{b}|n\rangle = n|n\rangle$. As the ground-state is then the vacuum of the Bogoliubons, $|\psi_{\text{gs}}\rangle_{\text{bog}} = |0\rangle$, then consequently the ground-state of the paramagnetic phase in the original Holstein-Primakoff bosons is the squeezed vacuum [10],

$$|\psi_{\text{GS}}\rangle_{\text{HP}} = \frac{1}{\sqrt{\cosh(r)}} \sum_{n=0}^{\infty} \tanh(r)^n \frac{\sqrt{(2n)!}}{2^n n!} |2n\rangle. \quad (50)$$

2. MQC spectrum

The MQC spectrum of the ground-state in the paramagnetic phase of the LMG model can be computed exactly using the result of $|\psi_{\text{GS}}\rangle_{\text{HP}}$. Specifically, the spectrum with respect to the basis of \hat{S}_x can be computed via the mapping $\hat{S}_x = \frac{N}{2} - \hat{a}^\dagger \hat{a}$, and using the definition of the MQC intensities in terms of the Fourier series

$$F_\phi \equiv |\langle \psi_{\text{GS}} | e^{-i\phi \hat{S}_x} | \psi_{\text{GS}} \rangle|^2 = \sum_m I_m^{\hat{S}_x}(\hat{\rho}_{\text{GS}}) e^{-im\phi}. \quad (51)$$

The LHS is solved upon substitution of Eq. (50) and we can then identify by inspection:

$$\begin{aligned} I_m^{\hat{S}_x}(\hat{\rho}_{\text{GS}}) &= \frac{m!}{2^m [(m/2)!]^2} \\ &\times {}_2F_1\left(\frac{1}{2}, \frac{1+m}{2}; \frac{2+m}{2}; \tanh(r)^4\right) \tanh(r)^m, \end{aligned} \quad (52)$$

where ${}_2F_1(a, b; c; x)$ is a hypergeometric function. Equation (52) is plotted in Fig. 2 of the main text for $m = 0, 2$.

The QPT is signalled by a vanishing of the MQC intensities as the approach the critical point $(\Omega/\chi)_c = 1$ from the paramagnetic phase. Specifically, Eq. (52) can be expanded in the vicinity of $(\Omega/\chi)_c = 1^+$ as

$$\begin{aligned} I_m^{\hat{S}_x}(\hat{\rho}_{\text{GS}}) \Big|_{\frac{\Omega}{\chi} \rightarrow 1^+} &\approx \frac{2}{\pi} \sqrt{\frac{\Omega}{\chi} - 1} \left[2H_{\frac{m-1}{2}} - 2\log(2) \right. \\ &\quad \left. - \log\left(\frac{\Omega}{\chi} - 1\right) \right]. \end{aligned} \quad (53)$$

where $H_n = \sum_{k=1}^n (1/k)$ is the n th Harmonic number. We stress that even though $I_m^{\hat{S}_x}(\hat{\rho}_{\text{GS}}) \rightarrow 0$ as $(\Omega/\chi)_c \rightarrow 1^+$, the analytical solution explicitly preserves $\sum_m I_m^{\hat{S}_x}(\hat{\rho}_{\text{GS}}) = 1$ for $N \rightarrow \infty$ (as we have assumed in the original derivation of the ground-state).

For completeness, the QPT is also reflected in the divergence of the associated first derivative as $(\Omega/\chi)_c \rightarrow 1^+$

$$\begin{aligned} \frac{dI_m^{\hat{S}_x}(\hat{\rho}_{\text{GS}})}{d\Omega} \Big|_{\frac{\Omega}{\chi} \rightarrow 1^+} &\approx \frac{-1}{\pi \sqrt{\frac{\Omega}{\chi} - 1}} \left[2 + 2H_{\frac{m-1}{2}} \right. \\ &\quad \left. + \log\left(4\left(\frac{\Omega}{\chi} - 1\right)\right) \right]. \end{aligned} \quad (54)$$

Finally, the MQC intensities can also be computed exactly for the ferromagnetic ground-state $|\psi_{\text{GS}}^F\rangle = (|(N/2)_z\rangle + |-(N/2)_z\rangle)/\sqrt{2}$ for arbitrary N . Specifically, using the identity

$$\begin{aligned} \langle (-N/2 + q)_z | e^{-i\phi \hat{S}_x} | (-N/2)_z \rangle &= \\ (-1)^q \sqrt{\frac{N!}{(N-q)!q!}} \cos^{N-q}(\phi/2) \sin^q(\phi/2) \end{aligned} \quad (55)$$

we obtain

$$|\langle \psi_{\text{GS}}^F | e^{-i\phi \hat{S}_x} | \psi_{\text{GS}}^F \rangle|^2 = \cos^{2N}(\phi/2) + \sin^{2N}(\phi/2) + 2^{1-N} \sin^N(\phi), \quad (56)$$

and

$$I_m^{\hat{S}_x}(\rho_{\text{GS}}^F) = \frac{2}{4^N} \binom{2N}{N-m} + \frac{2(-1)^{\frac{m}{2}}}{4^N} \binom{N}{\frac{N-m}{2}} \quad (57)$$

for m even and $I_m^{\hat{S}_x}(\rho_{\text{GS}}^F) = 0$ otherwise.

-
- [1] P. Richerme, C. Senko, S. Korenblit, J. Smith, A. Lee, R. Islam, W. C. Campbell, and C. Monroe, *Phys. Rev. Lett.* **111**, 100506 (2013).
 - [2] S. Balasubramanian, S. Han, B. T. Yoshimura, and J. K. Freericks, *Phys. Rev. A* **97**, 022313 (2018).
 - [3] R. J. Lewis-Swan, A. Safavi-Naini, J. J. Bollinger, and A. M. Rey, *Nature Communications* **10**, 1581 (2019).
 - [4] S. L. Braunstein and C. M. Caves, *Phys. Rev. Lett.* **72**, 3439 (1994).
 - [5] M. Gärttner, P. Hauke, and A. M. Rey, *Phys. Rev. Lett.* **120**, 040402 (2018).
 - [6] K. Macieszczak, E. Levi, T. Macrì, I. Lesanovsky, and J. P. Garrahan, *Phys. Rev. A* **99**, 052354 (2019).
 - [7] P. de Gennes, *Solid State Communications* **1**, 132 (1963).
 - [8] I. S. Gradshteyn and I. M. Ryzhik, *Table of Integrals, Series, and Products*, 7th ed. (Academic Press, San Diego, California, 2007).
 - [9] H.-M. Kwok, W.-Q. Ning, S.-J. Gu, and H.-Q. Lin, *Phys. Rev. E* **78**, 032103 (2008).
 - [10] D. F. Walls and G. J. Milburn, *Quantum Optics*, 2nd ed. (Springer, 2008).